Materials Advances

ROYAL SOCIETY OF CHEMISTRY

PAPER

View Article Online
View Journal | View Issue

Cite this: *Mater. Adv.*, 2022, 3, 4684

Synthesis of highly stable double-coated Zn-doped cesium lead bromide nanocrystals for indium ion detection in water†

Smaranika Ray, Ashutosh Mohapatra and Saikat Bhaumik *

Cesium lead halide ($CsPbX_3$: X = I, Br, Cl) perovskite nanocrystals (NCs) have proven their potential as a contender for various optoelectronic applications. They have also been used as fluorescent probes for the detection of different metal ions. However, perovskite NCs are prone to degradation by water, light, and heat. Therefore, it is essential to tackle these issues before implementing them in real-world applications. Recently, doping metal ions in perovskite structures and core/shell nanostructure formation are some of the strategies that have been implemented to improve NC stability, which is still not satisfactory. To further enhance NC stability, we grew a polyvinylpyrrolidone (PVP) polymer shell around pre-synthesized silica-coated Zn-doped $CsPbBr_3$ NCs, which demonstrated better stability against water and heat and less effectiveness in the halide exchange process. The optimized polymer shell around the NCs revealed the highest stability with improved emission intensity. The as-synthesized NCs were green emitters and showed maximum photoluminescence quantum yield (PLQY) up to 88%. The water and heat stability of the double-coated Zn-doped $CsPbBr_3$ NCs were increased by about two times compared with those of the silica-coated NCs. To the best of our knowledge, there are no reports to date on indium (In) ion detection using perovskite NCs as the fluorescent probe. Here, double-coated perovskite NCs were tested as a fluorescent probe for In ion detection in water. These observations are incredibly beneficial for lighting applications and can be used for In-ion detection in natural resources and industrial wastes.

Received 9th March 2022,
Accepted 25th April 2022

DOI: 10.1039/d2ma00272h

rsc.li/materials-advances

Introduction

All inorganic cesium lead halide ($CsPbX_3$: X = I, Br, Cl) perovskite nanocrystals (NCs) have emerged as promising materials for various optoelectronic applications due to their excellent properties, such as high absorption coefficient, color tunability, high luminescence intensity, narrow emission spectra, higher color purity, low threshold energy for lasing, and easy solution processability.[1–8] The photophysical properties of the NCs immensely depend on the interface between the outermost atoms and surface-bound passivating ligands.[9–11] If the outermost atoms are not fully passivated, they will create nonradiative defect/trap states, leading to low photoluminescence (PL) performance. The low activation energy of halide ion migration facilitates rapid phase segregation in mixed halide perovskites, unable to maintain their initial emission properties.[12–14] Such halide migration causes the formation of defect/trap states inside the perovskite structure, leading to the nonradiative recombination of charge carriers and resulting in poor emission intensity. The lower stability of perovskite crystal structures against water, light, and heat, is occurred due to their ionic nature and large surface energy, which is still a bottleneck for practical applications.[14–17]

Perovskite NCs are usually synthesized *via* a hot-injection or ligand-assisted reprecipitation (LARP) synthesis approach.[1,2] Recently, various efforts have been made to further improve the stability and photoluminescence (PL) intensity of NCs during the synthesis process.[16,18,19] One of the methods is the partial replacement of Pb ions with different divalent metal ions (*e.g.*, Zn, Mn, Mg, *etc.*) in the perovskite structure.[20–25] Such doping in the perovskite structure significantly improves structural stability *via* enhancing the formation energy, leading to an increase in emission intensity. Usually, partial substitution with smaller metal ions reduces the Pb–X bond length and stabilizes the perovskite structure by reducing octahedral distortion. It leads to an increase in the values of the tolerance factor and formation energy, which improve the overall perovskite phase stability and thermal stability. Zn-doped $CsPbX_3$ NCs have recently been employed in various optoelectronic devices for their improved crystal quality and reduced defect states.[21–23] Coating of perovskite NCs with comparatively stable

Institute of Chemical Technology-IndianOil Odisha Campus, Mouza-Samantapuri, Bhubaneswar, Odisha, India 751013. E-mail: s.bhaumik@iocb.ictmumbai.edu.in

† Electronic supplementary information (ESI) available. See DOI: https://doi.org/10.1039/d2ma00272h

shells, such as lower-dimensional perovskites [*e.g.*, $(OA)_2PbBr_4$, Cs_4PbX_6], metal oxides (*e.g.*, SiO_2, TiO_2), and metal sulfides (*e.g.*, ZnS, PbS), help improve NC stability and emission intensity, and resist ion migration among the NCs.[26–34]

Compared with the rigid inorganic shell, polymers are much more flexible and increase the hydrophobicity of the core NCs, thereby improving their water stability. Surface coating of perovskite NCs with bulky polymers [*e.g.*, poly(methyl methacrylate) (PMMA), polyhedral oligomeric silsesquioxane (POSS), polyvinylpyrrolidone (PVP), and polystyrene (PS)] enhance NC stability and improve dispersivity in different polar solvents.[26,27,35–37] SiO_2-coated perovskite NCs are also used in various applications due to their better stability in polar solvents.[21,38–41] Usually, water and alcohol originate from the hydrolysis and condensation processes of silica, which can attack perovskite NCs and generate surface defects.[42] The thin SiO_2 shell provides the core perovskite materials with limited stability in polar solvents, resulting in PL quenching. The growth of thicker SiO_2 shells is also a challenging process, and the NCs degrade very quickly during the coating process. Double-shell growth around the perovskite NCs proves to be an efficient method to improve NC stability further. Li *et al.* synthesized $CsPbBr_3/SiO_2/Al_2O_3$ core/shell/shell monoliths by incorporating $CsPbBr_3$ NCs into a SiO_2/Al_2O_3 monolith through a sol–gel process, demonstrating high stability and PLQY up to 90%.[43] $CsPbBr_3/TiO_2$/polymer nanosheets, $CsPbBr_3/SiO_2/ZrO_2$ nanocomposites, and $CsPbBr_3/SiO_2/SiO_2$ NCs with core/shell/shell structures also show better thermal, photo, and moisture stability.[42,44–47]

Indium tin oxide (ITO) is mainly utilized in semiconductor industries as a transparent conducting electrode for LEDs, televisions, solar cells, and other electronic devices.[48,49] The consumption of indium (In) is increasing rapidly worldwide. Since In is not an essential element for the function of the human body, overexposure to In-based compounds has potential health risks.[50,51] Therefore, accessible, cheap, sensitive, and real-time monitoring methods for detecting In ions are essential. Very few polymers have been tested as fluorescent probes for detecting In-ions.[52–54] Recently, perovskite NCs have been demonstrated as efficient fluorophores for the detection of different metal ions (*e.g.*, Cu, Hg, Zn) due to their high signal-to-noise ratio.[55–59] In this study, we have synthesized silica-coated Zn-doped $CsPbBr_3$ NCs *via* the LARP synthetic approach under normal atmospheric conditions (relative humidity above 80%). Then, we added different amounts of PVP polymer to grow different thick shells around the NCs and investigated their photophysical properties. We noticed that the PVP polymer-coating improves the overall NC stability and emission intensity. These observations encouraged us to investigate these double-coated Zn-doped $CsPbBr_3$ NCs as the fluorescent probe for In-ion detection in water.

Experimental section

Materials

Cesium bromide (CsBr, 99.999% trace metal basis), lead(II) bromide ($PbBr_2$, 99.999% trace metal basis), zinc bromide ($ZnBr_2$, 99.9%, trace metal basis), *N*,*N*′-dimethylformamide (DMF, anhydrous, 99.8%), tetrabutylammonium chloride (TBA-Cl, $\geq$97%), (3-aminopropyl)trimethoxysilane (APTMS, 97%), poly(vinyl pyrrolidone) (PVP, avg. $M_n \sim 6000$, PDI $\leq$ 1.2), and toluene (anhydrous, 99.8%) were purchased from Sigma Aldrich. *n*-Octylammonium bromide (OABr, 99%) was purchased from Greatcell Solar Materials. Ethanol (absolute for analysis, 99%) was purchased from Merck. Aluminum(III) chloride hydrate (97%, AR Grade) and potassium hydroxide (85%, pellets) were purchased from SD Fine Chem Limited. Iron(III) chloride (anhydrous, 98%) and calcium hydroxide (85%, pellets) were purchased from Avra Synthesis Private Limited. Iron(II) chloride hydrate (95%), indium(III) acetate (99.99%), cobalt nitrate (97%), and nickel(II) chloride hexahydrate (98%) were purchased from Central Drug House Private Limited, Alfa Aesar, Nice Chemicals Private Limited, and Sisco Research Laboratories Private Limited, respectively. All chemicals were used without further purification.

Synthesis of silica-coated Zn-doped $CsPbBr_3$ NCs

Silica-coated Zn-doped $CsPbBr_3$ NCs were synthesized *via* the ligand-assisted re-precipitation (LARP) method.[21] At first, in a glass vial, 0.016 mmol of CsBr, 0.004 mmol of OABr, 0.004 mmol $ZnBr_2$, and 0.02 mmol of $PbBr_2$ were mixed in 1.1 mL of DMF. The mixture was stirred at normal atmospheric conditions until a clear transparent solution was formed. Then, 10 μL of APTMS was mixed and shaken to form the final precursor solution. Then, 500 μL of the final precursor was swiftly injected into a round-bottomed glass flask containing 10 mL of toluene under normal atmospheric conditions. The mixture was continuously stirred for four hours to complete the hydrolysis process of APTMS to convert it into a compact silica shell around the NCs. After the completion of NC synthesis, the NC solution was transferred to a centrifuge tube and centrifuged at 3000 rpm for 10 min. Then, the supernatant was discarded, and the precipitate was dispersed in ethanol for further synthesis or characterization.

Post-synthesis treatment of silica-coated Zn-doped $CsPbBr_3$ NCs with PVP polymer

The Post-synthetic PVP treatment was carried out by adding 1 mL of diluted ($\sim$10 mg mL^{-1}) silica-coated Zn-doped $CsPbBr_3$ NCs to different amounts of PVP polymer (*i.e.*, 2.5 mg, 5 mg, 7.5 mg, and 10 mg) separately in round-bottomed glass flasks. The NCs were kept under continuous stirring conditions for six hours for the adsorption of PVP on the silica surface. The as-prepared NC solution was transferred to a centrifuge tube and centrifuged at 6000 rpm for 15 min. Then, the precipitate was collected and dispersed in ethanol for further characterization.

Preparation of the TBA-Cl precursor solution

The TBA-Cl precursor solution was prepared by dissolving 1 mmol of TBA-Cl salt (278 mg) in 5 mL toluene. The mixture was sonicated to dissolve the salt properly in the solvent.

Results and discussion

The schematic of the post-synthetic PVP coating of the silica-coated $CsPbBr_3$ NCs is shown in Fig. 1(a). PVP is a kind of non-ionic surfactant that can be adsorbed onto the surface of silica-coated NCs. The carbonyl or carboxyl group present in the organic PVP polymer chains can form hydrogen bonds with the hydroxyl groups present in the inorganic silica shell, which are formed after the complete hydrolysis of the silane precursor.[60,61] The absorption and PL spectra of the different polymer-coated Zn-doped $CsPbBr_3/SiO_2$ core/shell NCs dispersed in ethanol are shown in Fig. 1(b) and (c), respectively. The absorption spectrum of NCs-0 revealed a band edge absorption peak at around 512 nm.[21] With the increase in PVP polymer, the band edge positions of the corresponding NCs were slightly blue-shifted. The emission peak position of PVP-0 NCs was at 515 nm (FWHM ~ 23 nm) with a PLQY of about 83%. With an increase in PVP polymer up to a certain limit (for PVP-5 NCs), the PL peak position blue-shifted slightly to 511 nm. The emission intensity of the NCs also increased, confirming effective passivation of the silica-coated surface by the PVP polymer. The maximum PLQY of 88% was achieved for PVP-5 NCs. A similar emission shift was noticed when a PEO polymer was used to passivate silica-coated $MAPbBr_3$ NCs.[41] Such passivation of NCs increases the confinement effect, and as a result, the PL peak slightly blue-shifts. The photographic images of the double-coated PVP-5 NCs under normal daylight and UV light are represented in Fig. S1 (see ESI†). Further increments in PVP polymer showed a detrimental effect on the emission properties, with the emission peak position slightly red-shifted to 513 nm and decreased PL intensity. Excess polymer incorporation has a detrimental effect on the NC emission properties and results in enormous lattice strain at the interfaces. Such lattice strain results in significant bond length alterations that can modify the electronic band energies and shift the bands to lower energy.[62–64] The subsequent observations are provided in Table 1 for better understanding.

Table 1 Optical properties of the different double-coated NCs

Name of the NCs	PL Peak Position (nm)	FWHM (nm)	PLQY (%)
PVP-0	515	23	83
PVP-2.5	513	23	85
PVP-5	511	23	88
PVP-7.5	513	23	86
PVP-10	513	23	82

The X-ray diffraction (XRD) patterns of all NCs in the thin-film form are represented in Fig. 2(a). The XRD diffraction pattern of the PVP-0 NCs revealed a monoclinic phase of the $CsPbBr_3$ crystal structure (PDF #00-18-0364).[21,65,66] The broader XRD peaks correlated their sizes to the nanoscale region. The characteristic XRD diffraction peaks at the angles of 14.9°, 21.3°, 26.2°, 30.4°, 34.3°, 37.4°, and 43.5° corresponded with the (001), (110), (111), (002), (210), (211), and (202) lattice planes, respectively. Moreover, the diffraction peaks of the NCs shifted slightly to higher angles compared with the pure $CsPbBr_3$ diffraction peaks due to the expansion of the perovskite crystal lattices caused by the substitution of Pb atoms with the smaller-sized Zn atoms. The XRD diffraction peak positions of the PVP-coated NCs remained unchanged, confirming their similar monoclinic $CsPbBr_3$ crystal structure. This emphasizes that the polymer coating around the silica-coated NCs did not influence the core perovskite structures due to the protection offered by the thicker silica shell. The crystal phase of $(OA)_2PbBr_4$ was not detected as a very thin shell layer may have formed around the $CsPbBr_3$ NCs.[21,29]

The transmission electron microscopy (TEM) images of double-coated PVP-5 NCs were obtained to confirm the size and shape of the NCs and are represented in Fig. 2(b). The TEM images revealed that PVP-5 NCs had an average particle size distribution of 14.8 ± 6.7 nm. The slightly blurred surface around the NCs indicated the formation of a comparatively less dense silica shell. The compact silica coating around the NCs

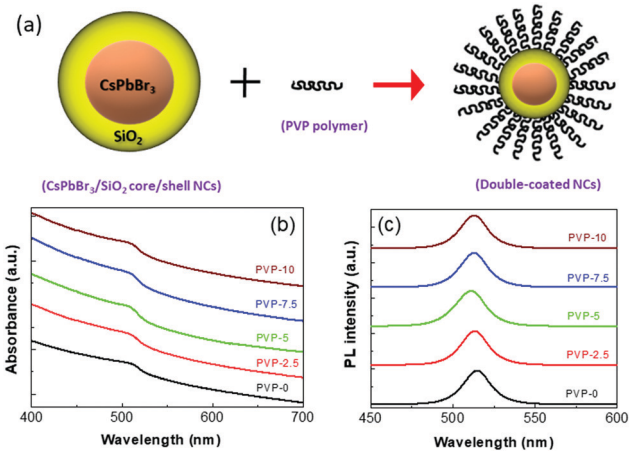

Fig. 1 (a) Schematic of PVP coating around the silica-coated $CsPbBr_3$ NCs. (b) Absorption and (c) PL spectra of different double-coated Zn-doped $CsPbBr_3$ NCs.

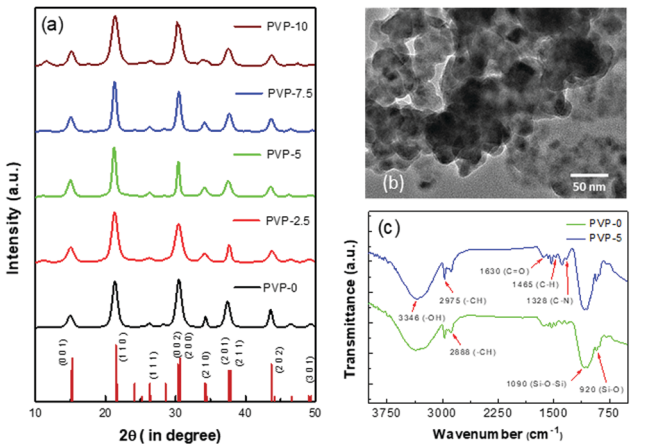

Fig. 2 (a) XRD diffraction patterns of the PVP-0, PVP-2.5, PVP-5, PVP-7.5, and PVP-10 NCs, as shown in the legend. The bottom of the figure represents the standard XRD diffraction patterns of the monoclinic $CsPbBr_3$ perovskite structure. (b) The TEM image of PVP-5 NCs. (c) FTIR spectra of PVP-0 and PVP-5 NCs, as shown in the legend.

protects them from the external harsh atmosphere. The TEM images of the other NCs are shown in Fig. S2a–d (see ESI† part). The NC images were not clear due to the presence of the thick and insulating PVP polymer, which causes a charging effect due to electron irradiation or possibly mechanical vibration of the tubes.[67] The HRTEM image of PVP-0 NCs revealed an interplanar spacing of 0.42 nm, which corresponded with the (001) lattice planes of the $CsPbBr_3$ monoclinic perovskite crystal phase (see Fig. S2e in ESI†).[21] We could not observe considerable changes in particle size distribution with the addition of the PVP shell. However, the NCs tended to agglomerate among themselves with higher amounts of the PVP polymer.[62,63]

We performed Fourier transform infrared (FTIR) spectroscopy analysis to confirm the presence of silica and PVP coating around the NCs. The FTIR spectra of the PVP-0 and PVP-5 NCs are shown in Fig. 2(c). The FTIR spectrum of PVP-0 NCs showed strong absorption peaks at 1090 and 920 cm^{-1} due to the asymmetric stretching vibration of the Si–O–Si bonds and symmetrical stretching vibration of the Si–O bonds, respectively.[21,38–40] The additional peak at 2888 cm^{-1} originated from the symmetric stretching vibration of the –CH bonds. These peaks confirmed the silica coating around the PVP-0 NCs. However, the FTIR spectrum of PVP-5 NCs showed enhanced characteristics peaks at 3346, 1630, and 1328 cm^{-1} originating from –OH bending, C═O stretching, and C–N stretching, respectively.[68–70] Some additional absorption peaks appeared at 2975 and 1465 cm^{-1} corresponding to strong C–H stretching and C–H bending, respectively, which confirmed the presence of the PVP polymer around the silica-coated NCs.[68–70] Therefore, these observations confirm that the polymer was deposited on the silica-coated perovskite NCs.

We performed the stability test of the different double-coated Zn-doped $CsPbBr_3$ NCs against the halide exchange process in the presence of the tetrabutylammonium chloride (TBA-Cl) precursor, and the corresponding observations are represented in Fig. 3(a)–(e). At first, the NC solutions at the same concentration (~5 mg mL^{-1}) were dispersed in 500 μL ethanol separately in quartz cuvettes. Then, we recorded the PL spectra of each NC solution before and after adding the TBA-Cl precursor solution. The corresponding observations were recorded at different time intervals, as shown in Fig. 3(f). The emission spectra of all the NCs were blue-shifted, and the emission intensity also decreased over time due to the fast anion exchange in $CsPbBr_3$ NCs caused by the substitution of the Br-ions with Cl-ions, which increased the overall bandgap of the resultant NCs.[71] The initial emission peak of PVP-0 NCs was at 518 nm, which blue-shifted by 57 nm after 18 min of reaction(see Fig. S3 in ESI†). The corresponding emission spectra of the PVP-2.5, PVP-5, PVP-7.5, and PVP-10 NCs were blue-shifted by 52, 48, 52, and 50 nm, respectively, with the addition of the same amount of TBA-Cl precursor. The halide exchange process was very fast upon the addition of TBA-Cl precursor inside the NC solutions, and it became slower over time.[12–14] Overall, these results indicate that the halide exchange process led to the deterioration of the optical properties of the NCs. However, it was noticed that, among all the samples, the PVP-5 NCs were less prone to the halide exchange reaction and presented better stability.

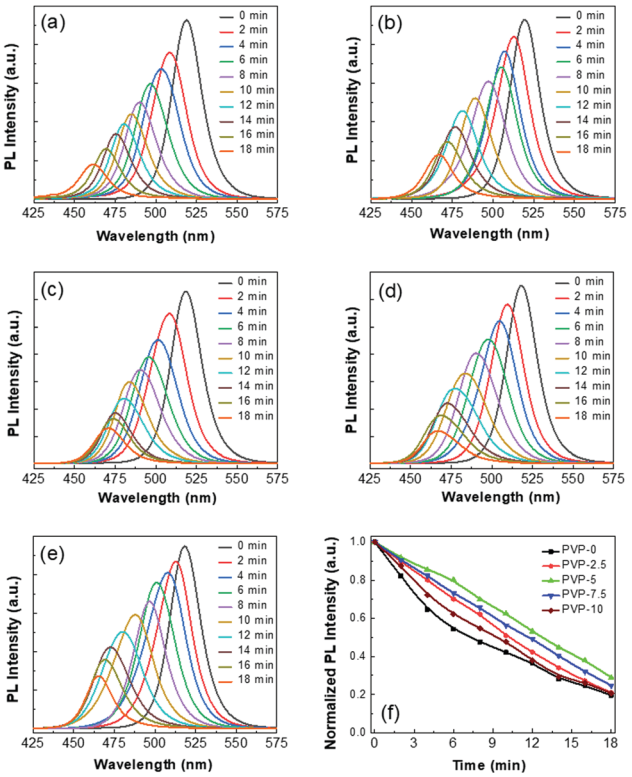

Fig. 3 PL spectra of the (a) PVP-0, (b) PVP-2.5, (c) PVP-5, (d) PVP-7.5, and (e) PVP-10 NCs after the addition of TBA-Cl precursor at different time intervals, as shown in the legend. (f) The decrease in the PL intensity of these NCs with time after halide exchange.

We performed a water stability test for all the NCs; the corresponding photographic images are represented in Fig. 4(a), and more detailed information can be seen in Fig. S4 (see ESI†). For this experiment, we took 100 μL of each NC solution in a glass vial and dispersed it in ethanol (concentration of ~10 mg mL^{-1}); then, we added 25 μL of deionized (DI) water in steps. The photographic images of the NC solutions were captured immediately after the addition of water and mixing in a vortex shaker. We recorded the volume of DI water required to change the NC emission properties under a UV lamp. We noticed that a certain amount of DI water was required for the emission of NCs to transform from green to blue color under the UV lamp due to the formation of comparatively stable blue-emitting lower-dimensional perovskite structures.[29,72] The UV-vis absorption and PL spectra of these blue-emitting NCs are shown in Fig. S5 (see ESI†), in which the absorption and PL peak positions are located at 461 and 470 nm, respectively. With the further addition of DI water to the NC solutions, the PL intensity was quenched due to the total degradation of the perovskite structures.[14–17] The photographic images of the different PVP-coated NC solutions under the UV lamp were captured when different amounts of DI water (0, 200 and 400 μL) were added (see Fig. 4(a)). We recorded the amount of DI water added to the NC solutions during these two

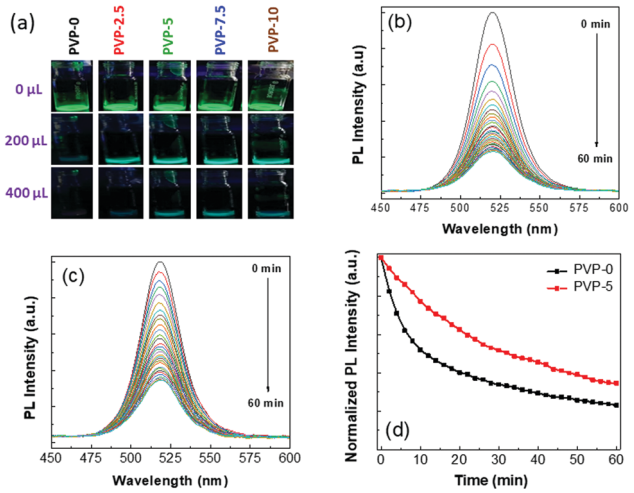

Fig. 4 (a) Water stability test: Photographic images of the PVP-0, PVP-2.5, PVP-5, PVP-7.5, and PVP-10 NC solutions under a UV lamp when different amounts of DI water (0, 200 and 400 μL) were added to the corresponding NC solutions. Heat stability test: PL spectra of the (b) PVP-0 and (c) PVP-5 NC films at different time periods. (d) The decrease in PL intensity of these films over time during the heat test, as shown in the legend.

transition points and tabulated these values in Table 2. From the table, it can be noticed that the emission color of PVP-0 NCs changed to blue with the addition of 200 μL DI water, and 280 μL DI water was required for total PL quenching. However, the polymer-coated NCs demonstrated better stability against water. Among them, PVP-7.5 NCs showed the best water stability, for which 375 and 475 μL of DI water were required for conversion to blue emission and total emission quenching of the NCs, respectively. These results indicate that the PVP polymer coating significantly improved the stability of the silica-coated Zn-doped $CsPbBr_3$ NCs.

High thermal stability is necessary for the practical application of perovskite NCs in conventional optoelectronic devices as the working temperatures are usually quite high.[73,74] Generally, the emission intensity of NCs falls significantly at higher temperatures due to the degradation of the perovskite structure, and the detachment of surface ligands causes the formation of surface trap states.[14–17] Therefore, we tested the heat stability of the PVP-0 and PVP-5 NC films heated at 100 °C under normal atmospheric conditions to understand the influence of the PVP polymer on NC stability (see Fig. S6 in ESI† part). We recorded the corresponding emission spectra of the NCs films at 2 min time intervals (see Fig. 4(b) and (c)). We noticed that the emission intensity of the PVP-0 NC film decreased much faster than the PVP-5 NC film. After 10 min of heating, the emission intensity of the PVP-0 and PVP-5 NC films retained ~52% and 77% of their initial PL intensity (see Fig. 4(d)), respectively, while no color change was observed under normal daylight. On prolonging the heating time up to 60 min, the emission intensity of the PVP-0 and PVP-5 NC films showed ~23% and 34% of their corresponding initial PL intensities. These results indicate that the polymer coating improved NC stability against heat.

Perovskite NCs have been proven as efficient Cu ion detectors.[55–57] Thus, we tried to detect different metal ions rather than only Cu ions and found that the perovskite NCs were capable of detecting In ions. The higher water and heat stability of the double-coated NCs inspired us to investigate their potential in In-ion detection in water. To perform this experiment, we first took 100 μL of the PVP-5 NC solution dispersed in ethanol (concentration ~5 mg mL^{-1}) in eight different glass vials. Then, we dropped equimolar aqueous solutions of Fe^{2+}, Fe^{3+}, Ca^{2+}, In^{3+}, K^{+}, Co^{2+}, Al^{3+}, and Ni^{2+}-ions in these glass vials separately. The photographic images of these NC solutions before and after the addition of metal ions under a UV lamp are shown in Fig. 5(a). We noticed that the emission intensity of one of these NC solutions with In^{3+}-ions was mostly quenched, while the emission intensity of the other solutions had slightly changed. The changes in the emission intensity of these NCs with the incorporation of different metal ions are shown in Fig. 5(b). They reveal effective In^{3+}-ion detection in water in the presence of the PVP-5 NCs. Later, we added In^{3+}-ion solutions at different concentrations (ranging from 0 to 104 μM) to the PVP-5 NC solution and recorded the corresponding emission spectra (see Fig. 5(c)). Here, the PL intensity first increased with the addition of a small amount of the In^{3+}-ion solution and then decreased monotonically with successive increases in the In^{3+}-ion concentration. However, the shape of the emission spectra remained almost unchanged and they did not shift to lower/higher wavelengths. Post-synthesis cation exchange with smaller size atoms in perovskite structure significantly improves structural stability *via* enhancing the formation energy, leading to an increase in emission intensity. We noticed that with the addition of a small amount of In^{3+}-ions (18 μM), the PL intensity of the NCs slightly increased and the PL spectrum also blue-shifted due to an increase in the bandgap energy, due to crystal lattice contraction or shrinkage caused by the substitution of Pb-ions with In-ions in the perovskite crystal lattices.[20–25] However, a linear

Table 2 Water stability test and shift in emission peak positions after halide exchange process of the different double-coated NCs

Name of the NCs	Volume of water required for emission color change from green to blue (μL)	Volume of water required for total PL quenching (μL)	Shift in emission peak position after the addition of TBA-Cl precursor (nm)
PVP-0	200	280	57
PVP-2.5	280	400	52
PVP-5	300	450	48
PVP-7.5	375	475	52
PVP-10	300	425	50

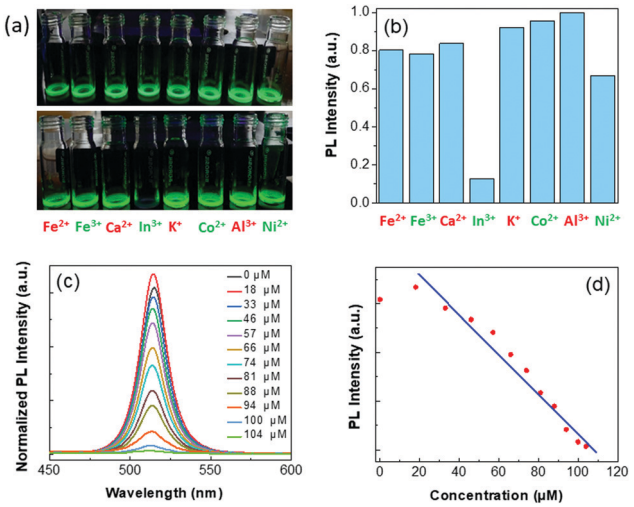

Fig. 5 (a) Photographic images of PVP-5 NC solutions under a UV lamp before (top) and after (bottom) the addition of different metal ions as marked at the bottom. (b) Chart representing the comparison of the PL intensity of PVP-5 NCs after the addition of different metal ions. (c) Emission spectra of PVP-5 NCs in the presence of different concentrations of In^{3+}-ions, as shown in the legend. (d) Linear fit (blue line) represents the decrease in the PL intensity of PVP-5 NCs after the addition of different concentrations of In^{3+}-ions.

decrease in PL intensity at higher concentrations of In^{3+}-ions was seen because of the trapping of charge carriers on the NC surface (see Fig. 5(d)).[56] Such surface modifications resulted in a decrease in NC PL intensity. We took the four lowest concentrations of In ions at which the PL intensity started changing and plotted the graph (see Fig. S7 in ESI†). We linear-fitted the points and calculated the detection limit by using the formula (3σ/slope).[52] The calculated value of the slope and σ (standard deviation) were obtained as 0.0046 and 0.0169, respectively. We calculated the detection limit as 11 μM (R^2 = 0.996) for In^{3+}-ions based on the slope and σ values. These observations verify the good In^{3+}-ion detection capability of double-coated Zn-doped $CsPbBr_3$ NCs in polar solvents with a broader probing window, which is helpful for In^{3+}-ion detection in natural and waste resources.

Conclusions

In summary, we report the coating of PVP polymer around pre-synthesized silica-coated Zn-doped $CsPbBr_3$ NCs under normal atmospheric conditions (humidity level above 80%) and investigated the effect of the polymer coating on the photophysical properties of the NCs. We found that the NCs crystallized into a monoclinic $CsPbBr_3$ perovskite crystal structure. The polymers did not have any effects on NC crystallinity. With optimized PVP coating, the NCs showed superior stability, dispersivity, and emission properties due to effective coating. Among them, the PVP-5 and PVP-7.5 NCs showed maximum stability and higher emission intensities. These NCs exhibited green emissions with a maximum PLQY of up to 88%. However, excess polymer incorporation led to agglomeration of the NCs and created trap states, which resulted in detrimental effects. The higher stability of these double-coated Zn-doped $CsPbBr_3$ NCs in polar solvents enabled them to detect In^{3+}-ions in water, with good detection capability in a broader probing window. These results are very promising for lighting applications, as well as ion detection in natural resources and industrial wastes.

Author contributions

S. B. conceived the research idea and planned the experiments accordingly. S. R. and A. M. performed the synthesis, characterization, and related experiments. The manuscript was written through contributions from all authors. All authors have given approval to the final version of the manuscript.

Conflicts of interest

There are no conflicts to declare.

Acknowledgements

S. B. acknowledges to Department of Science and Technology (DST), India (Award number# DST/INSPIRE/04/2017/000530) and Science and Engineering Research Board (SERB), India (Award number# SRG/2019/000093) for the financial assistance. We also acknowledge ICT-IOC start-up research grant for the financial support.

Notes and references

1 M. V. Kovalenko, L. Protesescu and M. I. Bodnarchuk, Properties and potential optoelectronic applications of lead halide perovskite nanocrystals, *Science*, 2017, **358**, 745–750.
2 Q. A. Akkerman, G. Rainò, M. V. Kovalenko and L. Manna, Genesis, challenges and opportunities for colloidal lead halide perovskite nanocrystals, *Nat. Mater.*, 2018, **17**, 394–405.
3 S. Yakunin, L. Protesescu, F. Krieg, M. I. Bodnarchuk, G. Nedelcu, M. Humer, G. De Luca, M. Fiebig, W. Heiss and M. V. Kovalenko, Low-threshold amplified spontaneous emission and lasing from colloidal nanocrystals of caesium lead halide perovskites, *Nat. Commun.*, 2015, **6**, 8056.
4 A. Swarnkar, A. R. Marshall, E. M. Sanehira, B. D. Chernomordik, D. T. Moore, J. A. Christians, T. Chakrabarti and J. M. Luther, Quantum dot-induced phase stabilization of α-$CsPbI_3$ perovskite for high-efficiency photovoltaics, *Science*, 2016, **354**, 92–95.
5 X.-K. Liu, W. Xu, S. Bai, Y. Jin, J. Wang, R. H. Friend and F. Gao, Metal halide perovskites for light-emitting diodes, *Nat. Mater.*, 2021, **20**, 10–21.
6 D. Liu, Y. Guo, M. Que, X. Yin, J. Liu, H. Xie, C. Zhang and W. Que, Metal halide perovskite nanocrystals: Application in high-performance photodetectors, *Mater. Adv.*, 2021, **2**, 856–879.
7 Y.-H. Kim, S. Kim, A. Kakekhani, J. Park, J. Park, Y.-H. Lee, H. Xu, S. Nagane, R. B. Wexler, D.-H. Kim, S. H. Jo, L. Martínez-Sarti, P. Tan, A. Sadhanala, G.-S. Park,

Y.-W. Kim, B. Hu, H. J. Bolink, S. Yoo, R. H. Friend, A. M. Rappe and T.-W. Lee, Comprehensive defect suppression in perovskite nanocrystals for high-efficiency light-emitting diodes, *Nat. Photonics*, 2021, **15**, 148–155.

8 Y. Wei, Z. Cheng and J. Lin, An overview on enhancing the stability of lead halide perovskite quantum dots and their applications in phosphor-converted LEDs, *Chem. Soc. Rev.*, 2019, **48**, 310–350.

9 J. De Roo, M. Ibáñez, P. Geiregat, G. Nedelcu, W. Walravens, J. Maes, J. C. Martins, I. Van Driessche, M. V. Kovalenko and Z. Hens, Highly dynamic ligand binding and light absorption coefficient of cesium lead bromide perovskite nanocrystals, *ACS Nano*, 2016, **10**, 2071–2081.

10 K. Hills-Kimball, H. Yang, T. Cai, J. Wang and O. Chen, Recent advances in ligand design and engineering in lead halide perovskite nanocrystals, *Adv. Sci.*, 2021, **8**, 2100214.

11 H. Ding, H. Jiang and X. Wang, How organic ligands affect the phase transition and fluorescent stability of perovskite nanocrystals, *J. Mater. Chem. C*, 2020, **8**, 8999–9004.

12 P. V. Kamat and M. Kuno, Halide ion migration in perovskite nanocrystals and nanostructures, *Acc. Chem. Res.*, 2021, **54**, 520–531.

13 C. Jia, H. Li, L. Tan, X. Meng, J. Gao and H. Li, Observation and implication of halide exchange beyond $CsPbX_3$ perovskite nanocrystals, *Nanoscale*, 2019, **11**, 3123–3128.

14 H. Zhang, X. Fu, Y. Tang, H. Wang, C. Zhang, W. W. Yu, X. Wang, Y. Zhang and M. Xiao, Phase segregation due to ion migration in all-inorganic mixed-halide perovskite nanocrystals, *Nat. Commun.*, 2019, **10**, 1088.

15 S. Seth, T. Ahmed, A. De and A. Samanta, Tackling the defects, stability, and photoluminescence of $CsPbX_3$ perovskite nanocrystals, *ACS Energy Lett.*, 2019, **4**, 1610–1618.

16 H. Huang, M. I. Bodnarchuk, S. V. Kershaw, M. V. Kovalenko and A. L. Rogach, Lead halide perovskite nanocrystals in the research spotlight: Stability and defect tolerance, *ACS Energy Lett.*, 2017, **2**, 2071–2083.

17 K. Xing, S. Cao, X. Yuan, R. Zeng, H. Li, B. Zou and J. Zhao, Thermal and photo stability of all inorganic lead halide perovskite nanocrystals, *Phys. Chem. Chem. Phys.*, 2021, **23**, 17113–17128.

18 D. Yang, X. Li and H. Zeng, Surface Chemistry of All Inorganic Halide Perovskite Nanocrystals: Passivation Mechanism and Stability, *Adv. Mater. Interfaces*, 2018, **5**, 1701662.

19 S. R. Smock, Y. Chen, A. J. Rossini and R. L. Brutchey, The Surface Chemistry and Structure of Colloidal Lead Halide Perovskite Nanocrystals, *Acc. Chem. Res.*, 2021, **54**, 707–718.

20 D. Chen, G. Fang, X. Chen, L. Lei, J. Zhong, Q. Mao, S. Zhou and J. Li, Mn-Doped CsPbCl3 perovskite nanocrystals: Solvothermal synthesis, dual-color luminescence and improved stability, *J. Mater. Chem. C*, 2018, **6**, 8990–8998.

21 M. R. Kar, R. Chakraborty, U. Patel, R. Chakraborty, S. Ray, T. K. Acharya, C. Goswami and S. Bhaumik, Impact of Zn-doping on the composition, stability, luminescence properties of silica coated all-inorganic cesium lead bromide nanocrystals and their biocompatibility, *Mater. Today Chem.*, 2022, **23**, 100753.

22 J. Li, J. Chen, L. Xu, S. Liu, S. Lan, X. Li and J. Song, A zinc non-halide dopant strategy enables efficient perovskite $CsPbI_3$ quantum dot-based light-emitting diodes, *Mater. Chem. Front.*, 2020, **4**, 1444–1453.

23 R. Wu, Q. Wang, S. Yang, L. Wu, S. Gong, Q. Han and W. Wu, Enhanced thermal stability of exciton recombination in $CsPbI_3$ perovskite nanocrystals *via* zinc alloying, *J. Alloys Compd.*, 2021, **857**, 157574.

24 Q. A. Akkerman, D. Meggiolaro, Z. Dang, F. De Angelis and L. Manna, Fluorescent alloy $CsPb_xMn_{1-x}I_3$ perovskite nanocrystals with high structural and optical stability, *ACS Energy Lett.*, 2017, **2**, 2183–2186.

25 S. Das, A. De and A. Samanta, Ambient condition Mg^{2+} doping producing highly luminescent green- and violet-emitting perovskite nanocrystals with reduced toxicity and enhanced stability, *J. Phys. Chem. Lett.*, 2020, **11**, 1178–1188.

26 M. R. Kar, S. Ray, B. K. Patra and S. Bhaumik, State of the art and prospects of metal halide perovskite core@shell nanocrystals and nanocomposites, *Mater. Today Chem.*, 2021, **20**, 100424.

27 S. Bera and N. Pradhan, Perovskite nanocrystal heterostructures: Synthesis, optical properties, and applications, *ACS Energy Lett.*, 2020, **5**, 2858–2872.

28 G. H. Ahmed, J. Yin, O. M. Bakr and O. F. Mohammed, Successes and challenges of core/shell lead halide perovskite nanocrystals, *ACS Energy Lett.*, 2021, **6**, 1340–1357.

29 S. Bhaumik, S. A. Veldhuis, Y. F. Ng, M. Li, S. K. Muduli, T. C. Sum, B. Damodaran, S. Mhaisalkar and N. Mathews, Highly stable, luminescent core–shell type methylammonium–octylammonium lead bromide layered perovskite nanoparticles, *Chem. Commun.*, 2016, **52**, 7118–7121.

30 V. K. Ravi, S. Saikia, S. Yadav, V. V. Nawale and A. Nag, $CsPbBr_3$/ZnS core/shell type nanocrystals for enhancing luminescence lifetime and water stability, *ACS Energy Lett.*, 2020, **5**, 1794–1796.

31 Z.-J. Li, E. Hofman, J. Li, A. H. Davis, C.-H. Tung, L.-Z. Wu and W. Zheng, Photoelectrochemically active and environmentally stable $CsPbBr_3/TiO_2$ core/shell nanocrystals, *Adv. Funct. Mater.*, 2018, **28**, 1704288.

32 J. Cai, K. Gu, Y. Zhu, J. Zhu, Y. Wang, J. Shen, A. Trinchi, C. Li and G. Wei, Highly stable $CsPbBr_3@SiO_2$ nanocomposites prepared *via* confined condensation for use as a luminescent ink, *Chem. Commun.*, 2018, **54**, 8064–8067.

33 C. Jia, H. Li, X. Meng and H. Li, $CsPbX_3/Cs4PbX_6$ core/shell perovskite nanocrystals, *Chem. Commun.*, 2018, **54**, 6300–6303.

34 X. Zhang, M. Lu, Y. Zhang, H. Wu, X. Shen, W. Zhang, W. Zheng, V. L. Colvin and W. W. Yu, PbS capped $CsPbI_3$ nanocrystals for efficient and stable light-emitting devices using p–i–n structures, *ACS Cent. Sci.*, 2018, **4**, 1352–1359.

35 H. Huang, B. Chen, Z. Wang, T. F. Hung, A. S. Susha, H. Zhong and A. L. Rogach, Water resistant $CsPbX_3$ nanocrystals coated with polyhedral oligomeric silsesquioxane and their use as solid state luminophores in all-perovskite white light-emitting devices, *Chem. Sci.*, 2016, **7**, 5699–5703.

36 Y. Liu, F. Li, L. Qiu, K. Yang, Q. Li, X. Zheng, H. Hu, T. Guo, C. Wu and T. W. Kim, Fluorescent microarrays of in situ crystallized perovskite nanocomposites fabricated for patterned

applications by using inkjet printing, *ACS Nano*, 2019, **13**, 2042–2049.

37 J. C. Yu, A.-Y. Lee, D. B. Kim, E. D. Jung, D. W. Kim and M. H. Song, Enhancing the performance and stability of perovskite nanocrystal light-emitting diodes with a polymer matrix, *Adv. Mater. Technol.*, 2017, **2**, 1700003.

38 F. Zhang, Z.-F. Shi, Z.-Z. Ma, Y. Li, S. Li, D. Wu, T.-T. Xu, X.-J. Li, C.-X. Shan and G.-T. Du, Silica coating enhances the stability of inorganic perovskite nanocrystals for efficient and stable down-conversion in white light-emitting devices, *Nanoscale*, 2018, **10**, 20131–20139.

39 D. Yan, T. Shi, Z. Zang, S. Zhao, J. Du and Y. Leng, Stable and low-threshold whispering-gallery-mode lasing from modified $CsPbBr_3$ perovskite quantum dots@SiO_2 sphere, *Chem. Eng. J.*, 2020, **401**, 126066.

40 A. Pan, Y. Li, Y. Wu, K. Yan, M. J. Jurow, Y. Liu and L. He, Stable luminous nanocomposites of $CsPbX_3$ perovskite nanocrystals anchored on silica for multicolor anti-counterfeit ink and white-LEDs, *Mater. Chem. Front.*, 2019, **3**, 414–419.

41 Y. He, Y. J. Yoon, Y. W. Harn, G. V. Biesold-McGee, S. Liang, C. H. Lin, V. V. Tsukruk, N. Thadhani, Z. Kang and Z. Lin, Unconventional route to dual-shelled organolead halide perovskite nanocrystals with controlled dimensions, surface chemistry, and stabilities, *Sci. Adv.*, 2019, **5**, eaax4424.

42 C. Rossi, R. Scarfiello, R. Brescia, L. Goldoni, G. Caputo, L. Carbone, D. Colombara, L. De Trizio, L. Manna and D. Baranov, Exploiting the transformative features of metal halides for the synthesis of $CsPbBr_3$@SiO_2 core–shell nanocrystals, *Chem. Mater.*, 2022, **34**, 405–413.

43 Z. Li, L. Kong, S. Huang and L. Li, Highly luminescent and ultrastable cspbbr3 perovskite quantum dots incorporated into a silica/alumina monolith, *Angew. Chem.*, 2017, **56**, 8134–8138.

44 Y. Duan, C. Ezquerro, E. Serrano, E. Lalinde, J. García-Martínez, J. R. Berenguer and R. D. Costa, Meeting high stability and efficiency in hybrid light-emitting diodes based on SiO2/ZrO_2 coated $CsPbBr_3$ perovskite nanocrystals, *Adv. Funct. Mater.*, 2020, **30**, 2005401.

45 V. Naresh, B. H. Kim and N. Lee, Synthesis of $CsPbX_3$ (X = Cl/Br, Br, and Br/I)@SiO_2/PMMA composite films as color-conversion materials for achieving tunable multi-color and white light emission, *Nano Res.*, 2021, **14**, 1187–1194.

46 Y. Huang, F. Li, L. Qiu, F. Lin, Z. Lai, S. Wang, L. Lin, Y. Zhu, Y. Wang, Y. Jiang and X. Chen, Enhancing the stability of $CH_3NH_3PbBr_3$ nanoparticles using double hydrophobic shells of SiO_2 and poly(vinylidene fluoride), *ACS Appl. Mater. Interfaces*, 2019, **11**, 26384–26391.

47 L. Qiu, H. Yang, Z. Dai, F. Sun, J. Hao, M. Guan, P. Dang, C. Yan, J. Lin and G. Li, Highly efficient and stable $CsPbBr_3$ perovskite quantum dots by encapsulation in dual-shell hollow silica spheres for WLEDs, *Inorg. Chem. Front.*, 2020, **7**, 2060–2071.

48 K. Zhang, Y. Wu, W. Wang, B. Li, Y. Zhang and T. Zuo, Recycling indium from waste LCDs: A review, *Resour., Conserv. Recycl.*, 2015, **104**, 276–290.

49 T. Minami, Present status of transparent conducting oxide thin-film development for indium-tin-oxide (ITO) substitutes, *Thin Solid Films*, 2008, **516**, 5822–5828.

50 A. Tanaka, M. Hirata, Y. Kiyohara, M. Nakano, K. Omae, M. Shiratani and K. Koga, Review of pulmonary toxicity of indium compounds to animals and humans, *Thin Solid Films*, 2010, **518**, 2934–2936.

51 T. Hamaguchi, K. Omae, T. Takebayashi, Y. Kikuchi, N. Yoshioka, Y. Nishiwaki, A. Tanaka, M. Hirata, O. Taguchi and T. Chonan, Exposure to hardly soluble indium compounds in ITO production and recycling plants is a new risk for interstitial lung damage, *Occup. Environ. Med.*, 2008, **65**, 51–55.

52 H. Cho, J. B. Chae and C. Kim, A thiophene-based blue-fluorescent emitting chemosensor for detecting indium(III) ion, *Inorg. Chem. Commun.*, 2018, **97**, 171–175.

53 P. K. Mehta, G. W. Hwang, J. Park and K.-H. Lee, Highly sensitive ratiometric fluorescent detection of indium(III) using fluorescent probe based on phosphoserine as a receptor, *Anal. Chem.*, 2018, **90**, 11256–11264.

54 C. Kim and J. B. Chae, A highly selective fluorescent chemosensor for detecting indium(III) with a low detection limit and its application, *J. Fluoresc.*, 2018, **28**, 1363–1370.

55 Q. Li, W. Zhou, L. Yu, S. Lian and Q. Xie, Perovskite quantum dots as a fluorescent probe for metal ion detection in aqueous solution *via* phase transfer, *Mater. Lett.*, 2021, **282**, 128654.

56 Y. Liu, X. Tang, T. Zhu, M. Deng, I. P. Ikechukwu, W. Huang, G. Yin, Y. Bai, D. Qu, X. Huang and F. Qiu, All-inorganic $CsPbBr_3$ perovskite quantum dots as a photoluminescent probe for ultrasensitive Cu^{2+} detection, *J. Mater. Chem. C*, 2018, **6**, 4793–4799.

57 X. Niu, H. Gao and J. Du, $CsPbBr_3$ perovskite nanocrystals decorated with cu nanoclusters for ratiometric detection of glucose, *ACS Appl. Nano Mater.*, 2022, **5**, 2350–2357.

58 J. Guo, S. Ye, J. Song and J. Qu, Large-scale synthesis of cesium lead halide perovskite nanocrystals for zinc ion detection, *J. Nanopart. Res.*, 2020, **22**, 153.

59 Y. Shu, L. Sun, Y. Wang, D. Jin, Q. Xu and X. Hu, Polymer surface ligand and silica coating induced highly stable perovskite nanocrystals with enhanced aqueous fluorescence for efficient Hg^{2+} and glutathione detection, *Analyst*, 2021, **146**, 6798–6807.

60 M. Liu, Q. Chen, S. Wang, L. Bai, M. Sang, W. Jiang, S. Xuan and X. Gong, PVP immobilized SiO_2 nanospheres for high-performance shear thickening fluid, *J. Nanopart. Res.*, 2017, **19**, 234.

61 G. J. Owens, R. K. Singh, F. Foroutan, M. Alqaysi, C.-M. Han, C. Mahapatra, H.-W. Kim and J. C. Knowles, Sol–gel based materials for biomedical applications, *Prog. Mater. Sci.*, 2016, **77**, 1–79.

62 S. Kango, S. Kalia, A. Celli, J. Njuguna, Y. Habibi and R. Kumar, Surface modification of inorganic nanoparticles for development of organic–inorganic nanocomposites: A review, *Prog. Polym. Sci.*, 2013, **38**, 1232–1261.

63 H. Yang, Q. Zhang, M. Guo, C. Wang, R. Du and Q. Fu, Study on the phase structures and toughening mechanism in PP/EPDM/SiO_2 ternary composites, *Polymer*, 2006, **47**, 2106–2115.

64 A. M. Smith and S. Nie, Semiconductor nanocrystals: Structure, properties, and band gap engineering, *Acc. Chem. Res.*, 2010, **43**, 190–200.

65 L. Xu, J. Li, T. Fang, Y. Zhao, S. Yuan, Y. Dong and J. Song, Synthesis of stable and phase-adjustable $CsPbBr_3$@Cs_4PbBr_6 nanocrystals *via* novel anion–cation reactions, *Nanoscale Adv.*, 2019, **1**, 980–988.

66 A. Alaei, A. Circelli, Y. Yuan, Y. Yang and S. S. Lee, Polymorphism in metal halide perovskites, *Mater. Adv.*, 2021, **2**, 47–63.

67 K. Hirahara, K. Saitoh, J. Yamasaki and N. Tanaka, Direct observation of six-membered rings in the upper and lower walls of a single-wall carbon nanotube by spherical aberration-corrected HRTEM, *Nano Lett.*, 2006, **6**, 1778–1783.

68 H. Zhang, X. Wang, Q. Liao, Z. Xu, H. Li, L. Zheng and H. Fu, Embedding perovskite nanocrystals into a polymer matrix for tunable luminescence probes in cell imaging, *Adv. Funct. Mater.*, 2017, **27**, 1604382.

69 L. Wang, C. Shen and Y. Cao, PVP modified Fe_3O_4@SiO_2 nanoparticles as a new adsorbent for hydrophobic substances, *J. Phys. Chem. Solids*, 2019, **133**, 28–34.

70 J.-T. Song, X.-Q. Yang, X.-S. Zhang, D.-M. Yan, M.-H. Yao, M.-Y. Qin and Y.-D. Zhao, Composite silica coated gold nanosphere and quantum dots nanoparticles for X-ray CT and fluorescence bimodal imaging, *Dalton Trans.*, 2015, **44**, 11314–11320.

71 Q. A. Akkerman, V. D'Innocenzo, S. Accornero, A. Scarpellini, A. Petrozza, M. Prato and L. Manna, Tuning the optical properties of cesium lead halide perovskite nanocrystals by anion exchange reactions, *J. Am. Chem. Soc.*, 2015, **137**, 10276–10281.

72 S. K. Ha, C. M. Mauck and W. A. Tisdale, Toward stable deep-blue luminescent colloidal lead halide perovskite nanoplatelets: Systematic photostability investigation, *Chem. Mater.*, 2019, **31**, 2486–2496.

73 W. Wondrak, Physical limits and lifetime limitations of semiconductor devices at high temperatures, *Microelectron. Reliab.*, 1999, **39**, 1113–1120.

74 K. Górecki and J. Zarębski, Modeling the influence of selected factors on thermal resistance of semiconductor devices, *IEEE Trans. Compon., Packag., Manuf. Technol.*, 2014, **4**, 421–428.